Electronic Supplementary Material (ESI) for RSC Advances.

Electronic Supplementary Information

Photophysical properties of betaxanthins: miraxanthin V – insight into the excited-state deactivation mechanism from the experiment and computations.

Stanisław Niziński,[a] Monika Wendel,[a] Michał F. Rode, *[b] Dorota Prukała,[c] Marek Sikorski,[c] Sławomir Wybraniec[d] and Gotard Burdziński *[a]

[a] Quantum Electronics Laboratory, Faculty of Physics, Adam Mickiewicz University in Poznań, Umultowska 85, Poznan, 61-614, Poland

[b] Institute of Physics, Polish Academy of Sciences, Aleja Lotników 32/46, 02-668 Warsaw, Poland

[c] Faculty of Chemistry, Adam Mickiewicz University in Poznań, Umultowska 89b, 61-614 Poznań, Poland

[d] Faculty of Chemical Engineering and Technology, Institute C-1, Section of Analytical Chemistry, Cracow University of Technology, Warszawska 24, 31-155 Cracow, Poland

* gotardb@amu.edu.pl, mrode@ifpan.edu.pl

Table S1. (A) Vertical excitation energies (ΔE), oscillator strengths (f) of the low-energy singlet excited states of miraxanthin V calculated with the B3LYP/aug-cc-pVDZ method at the geometries optimized for the ground electronic state at the B3LYP/cc-pVDZ level for the two stereoisomeric forms: ***EE*** and ***ZE*** (in vacuum, methanol and water). (B) ΔE for the dominant ***EE*** stereoisomer of miraxanthin V calculated at the B3LYP/6-311++G(3df,3pd) level of theory with polarizable continuum model (PCM) for water and methanol, for comparison.

(A)

	ΔE [eV]	**f**	**ΔE [nm]**	**μ[D]**
***EE*, in vacuum, ε=1.00, n=1.00**				
S_0	**0.00**			2.1
S_1(π–>π*)	3.09	0.2006	401	
S_2(π–>π*)	3.29	0.5252	377	
S_3(n–>π*)	3.76	0.0067	330	
S_4(n–>π*)	3.94	0.0004	315	
S_5(n–>π*)	4.05	0.0035	306	
S_6(π–>π*)	4.44	0.0124	279	
***EE*, in methanol, ε=32.613, n=1.33141**				
S_0	**0.00**			3.21
S_1(π–>π*)	3.08	0.6628	403	
S_2(π–>π*)	3.23	0.1432	384	
S_3(n–>π*)	3.92	0.0025	316	
S_4(n–>π*)	3.97	0.0014	313	
S_5(n–>π*)	4.29	0.0005	289	
S_6(π–>π*)	4.42	0.0219	280	
***EE*, in water, ε=78.3553, n=1.330**				
S_0	**0.00**			3.25
S_1(π–>π*)	3.08	0.6665	401	
S_2(π–>π*)	3.23	0.1394	383	
S_3(n–>π*)	3.93	0.0023	316	
S_4(n–>π*)	3.97	0.0015	313	
S_5(n–>π*)	4.30	0.0005	288	
S_6(π–>π*)	4.42	0.0222	281	
***ZE*, in vacuum, ε=1.00, n=1.00**				
S_0	**+0.17**			3.84
S_1(π–>π*)	2.94	0.0655	422	
S_2(π–>π*)	3.27	0.5354	379	
S_3(π–>π*)	3.40	0.0610	365	
S_4(n–>π*)	3.78	0.0002	328	
S_5(n–>π*)	4.09	0.0023	303	
S_6(π–>π*)	4.45	0.0242	279	
***ZE*, in methanol, ε=32.613, n=1.33141**				
S_0	**+0.20**			5.38
S_1(π–>π*)	3.04	0.3875	407	
S_2(π–>π*)	3.17	0.3378	391	
S_3(n–>π*)	3.63	0.0053	341	
S_4(n–>π*)	3.88	0.0005	319	
S_5(n–>π*)	4.30	0.0004	289	
S_6(π–>π*)	4.42	0.0238	281	
***ZE*, in water, ε=78.3553, n=1.330**				
S_0	**+0.20**			5.44
S_1(π–>π*)	3.05	0.4082	407	
S_2(π–>π*)	3.17	0.3166	390	
S_3(n–>π*)	3.64	0.0052	341	
S_4(n–>π*)	3.89	0.0005	319	
S_5(n–>π*)	4.31	0.0004	288	
S_6(π–>π*)	4.42	0.0234	281	

(B)

***EE*, in vacuum**		
	f	**ΔE [nm]**
S_1	0.3678	384
S_2	0.3521	374
S_3	0.0090	333
***EE*, in methanol**		
	f	**ΔE [nm]**
S_1	0.7549	395
S_2	0.0499	377
S_3	0.0061	323
***EE*, in water**		
	f	**ΔE [nm]**
S_1	0.7589	395
S_2	0.0474	377
S_3	0.0061	323

Table S2. Comparison of some important features of miraxanthin V, indicaxanthin and vulgaxanthin I in water.

Dye	τ_1,τ_2 [ps]	Φ_f [$\times 10^{-3}$]	Stokes shift [cm^{-1}]	$\lambda_{abs}^{max}\ S_1 \rightarrow S_n\ [nm]$
miraxanthin V	4.2, 24.2	3	1528	394
indicaxanthin	4.8, 27	5.3	1270	395
vulgaxanthin I	2.9, 37	7.3	1600	392

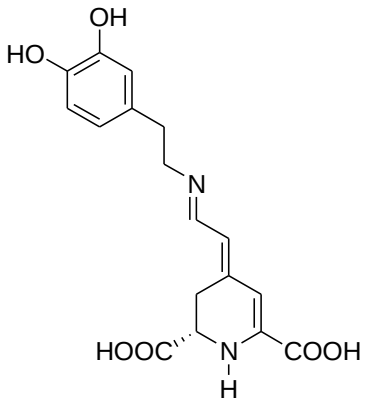

miraxanthin V

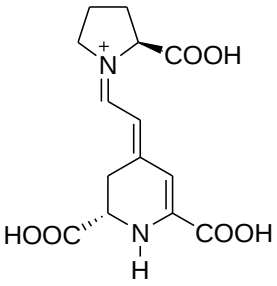

indicaxanthin

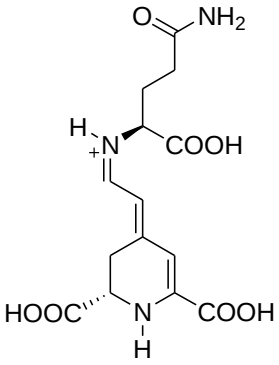

vulgaxanthin I

Table S3. Vertical excitation energies (ΔE, in eV), oscillator strengths ($f(S_0 \rightarrow S_n)$, $n \geq 1$) and dipole moments (μ, in Debye) of miraxanthin V calculated with the ADC2/cc-pVDZ method at the MP2/cc-pVDZ ground-state equilibrium geometries.

	ΔE [eV]	$f(S_0 \rightarrow S_n)$	μ [D]
EE			
S_0	0.00		2.8
$S_1(\pi \rightarrow \pi_A^*)$	3.70	0.750	4.9
$S_2(n \rightarrow \pi_A^*)$	4.37	0.010	6.5
$S_3(\pi \rightarrow \pi_D^*)$	4.80	0.083	2.9
$S_4(n\pi^*)$	4.87	0.0003	6.2
$S_5(\pi\pi^*)$	5.10	0.108	24.2
$S_6(\pi\pi^*)$	5.35	0.099	6.8
ZE			
S_0	+0.16		3.4
$S_1(\pi \rightarrow \pi_A^*)$	3.68	0.700	5.9
$S_2(n \rightarrow \pi_A^*)$	3.95	0.011	6.4
$S_3(\pi_D\pi_D^*)$	4.77	0.087	7.6
$S_4(n\pi^*)$	4.84	0.008	5.5
$S_5(n\pi^*)$	4.90	0.005	15.5
$S_6(\pi\pi^*)$	5.29	0.145	4.5

Table S4. Determined data for temperature-dependent transient absorption experiments of miraxanthin V in MeOH.

T [K]	Global analysis		PBI				NBI			
	τ_1 [ps]	τ_2 [ps]	τ_1 [ps]	τ_2 [ps]	$A_1/(A_1+A_2)$	$A_2/(A_1+A_2)$	τ_1 [ps]	τ_2 [ps]	$A_1/(A_1+A_2)$	$A_2/(A_1+A_2)$
182	15.4	219	38.7	297	0.39	0.61	37.8	296	0.38	0.62
195	9.4	153	30.1	218	0.4	0.6	31.4	229	0.41	0.59
205	7.5	120	20.2	155	0.38	0.62	22.6	166	0.39	0.61
206	6.5	110	18.1	137	0.22	0.78	17.5	140	0.38	0.62
220	5.2	83	15.5	105	0.37	0.63	21.7	123	0.43	0.57
222	5.2	81	14.4	96	0.36	0.64	16.2	106	0.38	0.62
238	4.2	59	10.3	67	0.33	0.67	7.5	67	0.31	0.69
239	3.0	58	10.2	69	0.32	0.68	14.4	79	0.37	0.63
249	3.1	44	9.2	55	0.34	0.66	16.5	70	0.47	0.53
260	2.1	40	11.4	55	0.37	0.63	11.9	60	0.41	0.59
269	2.7	32.4	7.7	41	0.36	0.64	8.7	43	0.4	0.6
285	2.3	25.5	5.8	30.4	0.31	0.69	7	34.2	0.39	0.61
286	1.9	29.2	4.8	33.4	0.32	0.68	5.8	37.4	0.35	0.65
295	1.4	20.9	5.8	27.6	0.3	0.7	7	31.3	0.39	0.61

Table S5. The most relevant HF/cc-pVDZ molecular orbitals involved in the $S_0 \rightarrow S_1$ transition determined for miraxanthin V at the equilibrium geometry of the ground state S_0 for the ***EE*** form (left panel) and for the ***ZE*** form (right).

	S_0.*EE*		**S_0.*ZE***	
LUMO (π*)	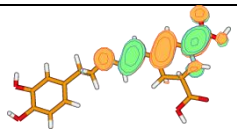 LUMO (92)		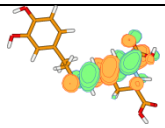 LUMO (92)	
HOMO (π)	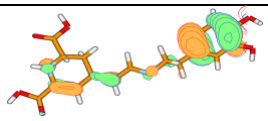 HOMO (90)	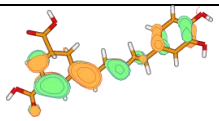 HOMO (91)	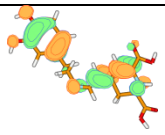 HOMO (90)	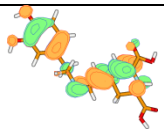 HOMO (91)
	= +0.86 (91a_92a) - 0.32 (90a_92a) (75 %) + (10 %)		= +0.72 (91a_92a) - 0.57 (90a_92a) (66 %) + (18 %)	

Table S6. Comparison of the geometric parameters (bond lengths, in Å), adiabatic energies (E^a, in eV), dipole moments (μ, in Debye) and oscillator strength ($f(S_1 \rightarrow S_0)$) for the equilibrium ground state (S_0) and the excited state (S_1) geometries optimized at the MP2/cc-pVDZ (for S_0) and the ADC2/cc-pVDZ (for S_1) levels of theory. The fluorescence energy (E_f, in eV) and oscillator strength $f(S_1 \rightarrow S_0)$ are given for the S_1-state.

	C_8-N_9	C_{10}=N_9	C_{10}-C_{11}	C_{11}=C_{12}	E_a [eV]	E_f [eV]	μ[D]	$f(S_1 \rightarrow S_0)$
S_0.*EZ*	1.456	1.298	1.456	1.374	0.04		3.6	
S_1.*EZ*. $\pi\pi^*$ 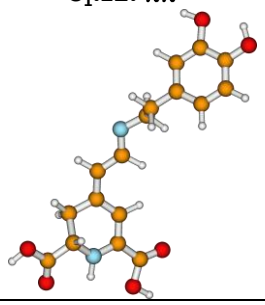	1.449	1.316	1.429	1.418	3.43	3.08	6.8	0.5539

Even though the ***EE*** and ***ZE*** forms were found to constitute the S_0-state equilibrium in experimental conditions, and other forms have much smaller contributions, one may try to optimize other stable conformers. One of them is the ***EZ*** form, which is a stereoisomer of the ***EE*** form with respect to the rotation about the C=C bond. Its geometry was optimized both in the ground and in the excited $\pi\pi^*$-state (see Table above). Both the ground and the excited-state geometry of the ***EZ*** form are found to be similar to the respective ***EE*** forms. The excited-state forms of both stereoisomers have similar photophysical properties, such as fluorescence energy, and are isoenergetic. That's why it can be assumed that the photophysics of those forms would be also similar.

Table S7. The most relevant HF/cc-pVDZ molecular orbitals involved in the $S_1 \rightarrow S_0$ nonadiabatic transition determined for miraxanthin V at the exemplary conical intersection geometry between the excited state, S_1, and the ground electronic state, S_0.

	CI(S_1/S_0)	
LUMO (π*)	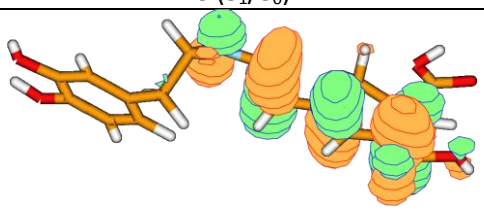 LUMO (92) π*	
HOMO (n / π)	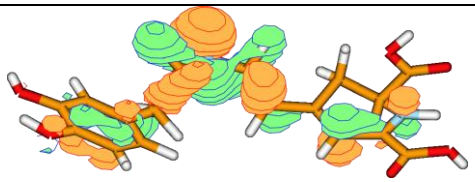 HOMO (88) n	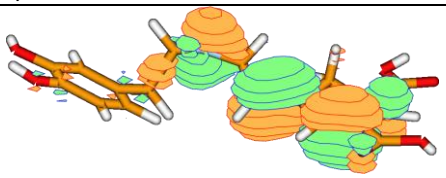 HOMO (91) π
	= +0.77 (88a_92a) + 0.51 (91a_92a)	
	= (61 %) + (26 %)	

Figure S1. (A) Normalized fluorescence spectrum of miraxanthin V in H_2O (λ_{exc} = 470 nm) obtained with larger 2 mm excitation and emission slits to improve signal-to-noise ratio. For a comparison, the reference data obtained in pure H_2O are also shown to indicate Raman contribution at $\lambda \approx 562$ nm. The fluorescence spectrum is weakly affected by Raman contribution, the corrected flurescence spectrum is very close to uncorrected data. (B) Normalized absorption and fluorescence excitation spectra (λ_f = 520 nm) of miraxanthin V in aqueous solution.

(A)

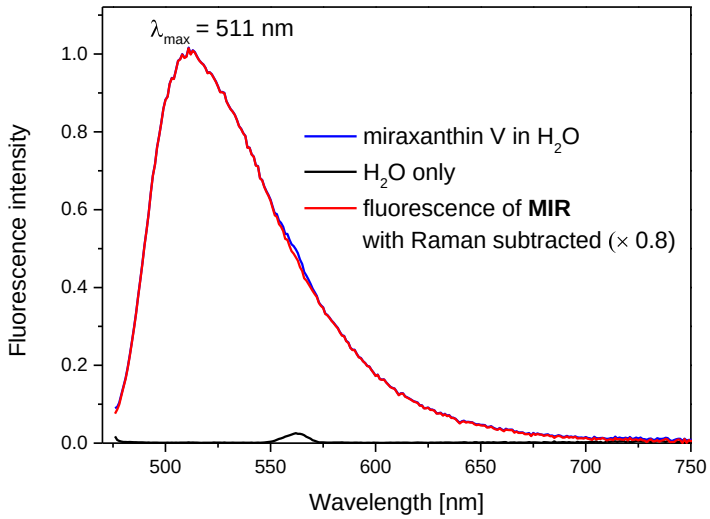

(B)

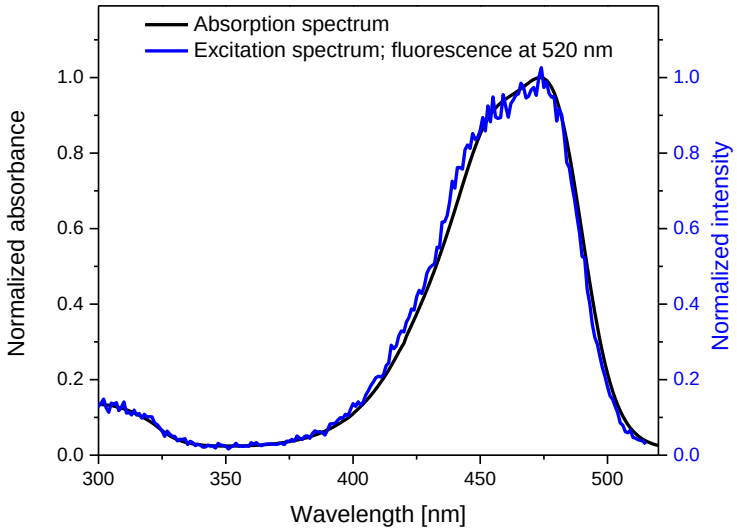

Figure S2. Contour plot of 3D fluorescence of miraxanthin V in water, recorded at right angle condition. (*) shows a weak solvent Raman contribution (OH band at 3400 cm^{-1}).

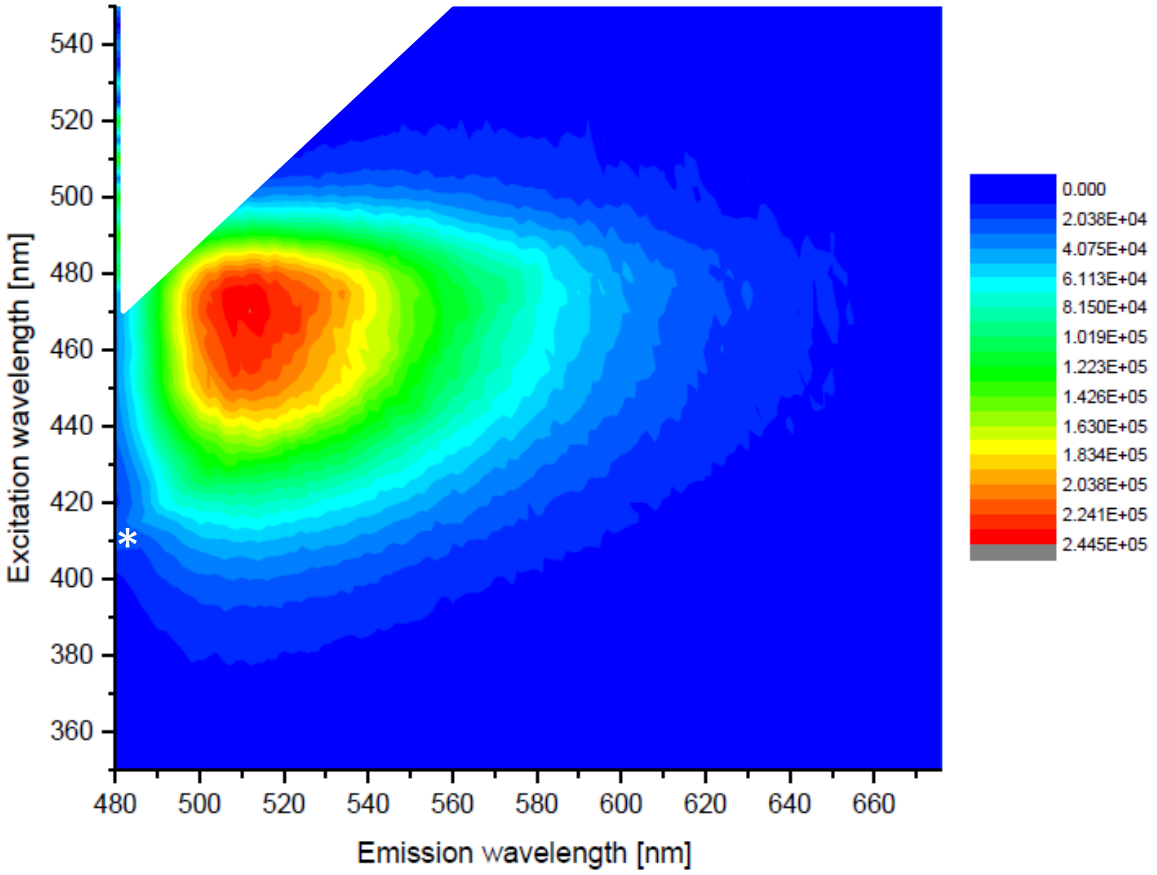

Figure S3. Effect of macroscopic solvent viscosity η on miraxanthin V fluorescence quantum yield Φ_f. A linear fit was performed for the dependence between $\ln(k_r/\Phi_f)$ and $\ln(\eta)$, as expected for a molecule with internal rotation in the excited state [Allen *et al.* Phys. Chem. Chem. Phys. 2005 (7) 3035]. The assumed value of radiative rate constant k_r is 2.2×10^8 s^{-1}.

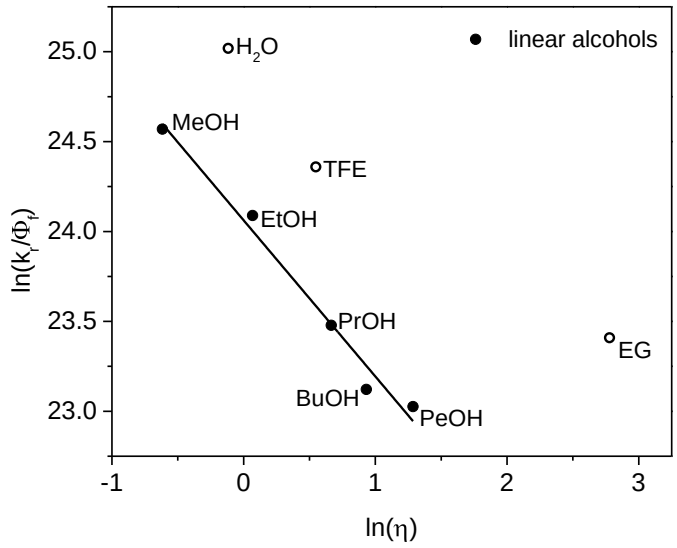

Figure S4. Normalized transient absorption spectra obtained for miraxanthin V in water (λ_{exc} = 480 nm).

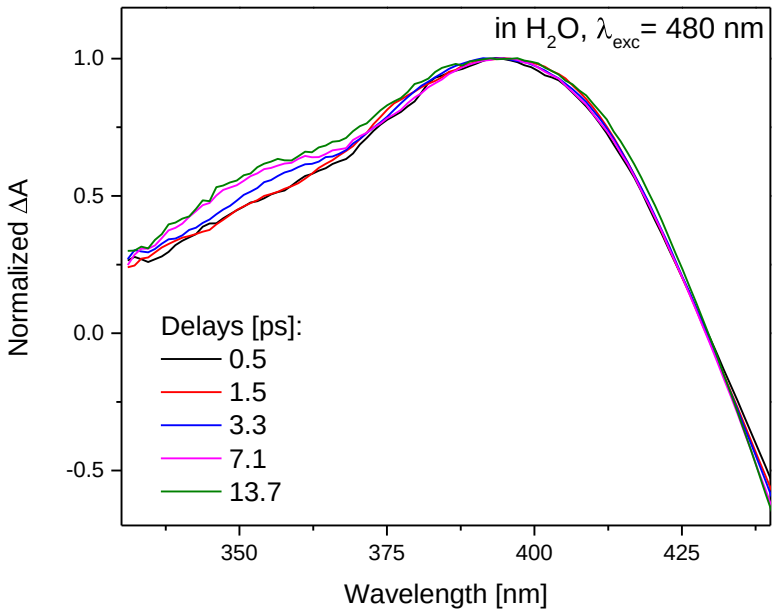

Figure S5. Band integral for miraxanthin V in water calculated over negative band (NBI), positive band (PBI) and both regions (EBI).

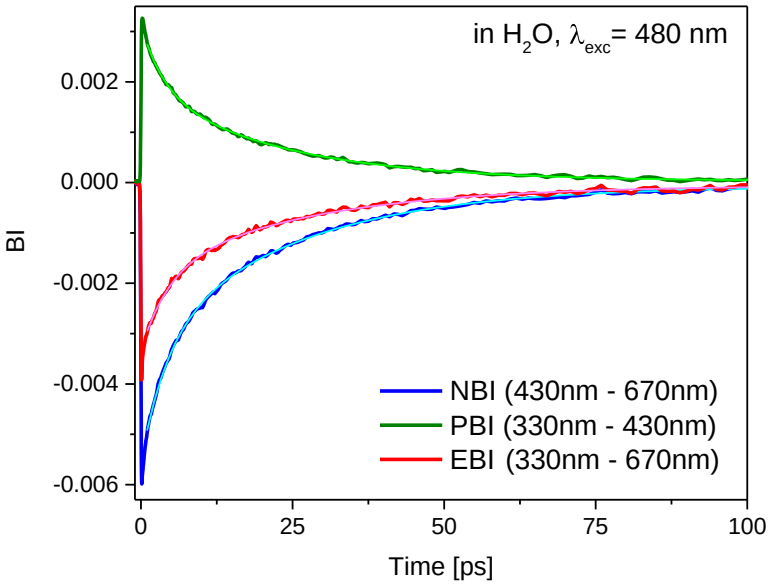

Figure S6. The relative amplitude A_1 of the short component in band integral kinetics (negative BI in Table 2) versus solvent polarity π^*.

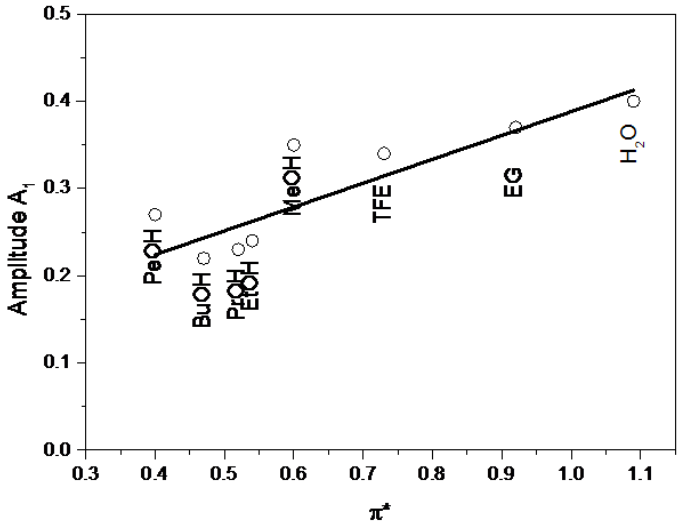

Figure S7. Transient absorption kinetic traces obtained for miraxanthin V in H_2O (λ_{exc} = 480 nm) at selected probe wavelengths. Fitting was performed with biexponential function

$$\Delta A = A_1 \exp(-t/\tau_1) + A_2 \exp(-t/\tau_2) + \text{offset}$$

convoluted with ~150 fs Gaussian IRF. Accuracy of the time-constant is ± 15 %.

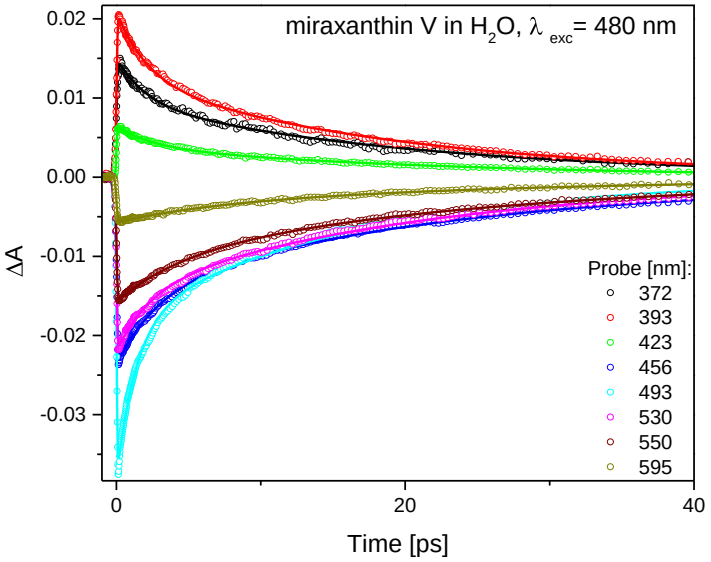

Probe [nm]	**A_1**	τ_1[ps]	**A_2**	τ_2[ps]	**Offset**
372	0.0056	2.0	0.0094	20.2	0.0001
393	0.0083	2.1	0.0125	18.7	0.0002
423	0.0026	2.6	0.0039	22.9	0
456	-0.0088	2.9	-0.0142	21.5	-0.0007
493	-0.0197	1.35	-0.0183	16.0	-0.0002
530	-0.0073	2.3	-0.0145	20.8	-0.0002
550	-0.0051	4.3	-0.0105	24.4	-0.0001
595	-0.0019	6.7	-0.0038	26.5	-0.0001

Figure S8. (A) NIR transient absorption spectra recorded in with excitation at 485 nm for miraxanthin V in water. (B) The determined decay-associated spectra with their respective time constants obtained by double-exponential global fit. (C) Two time constants τ_1 and τ_2 were obtained from double exponential fit of band integral: 2.7 ps (0.41) and 21.9 ps (0.59).

(A)

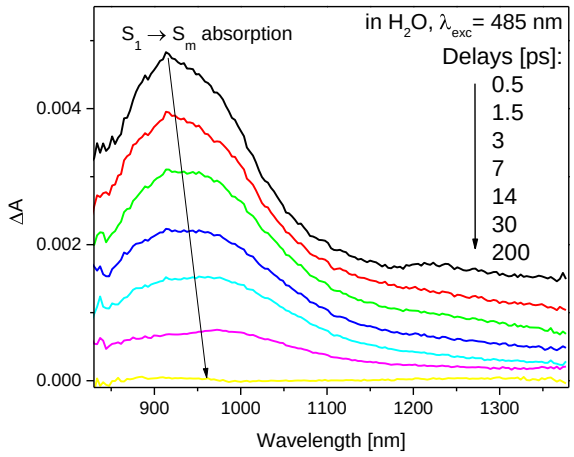

(B)

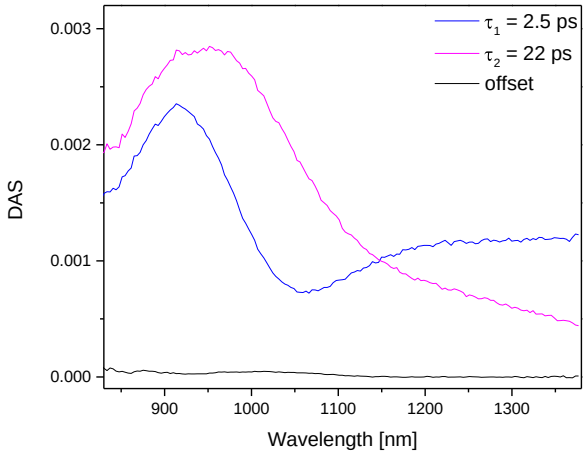

(C)

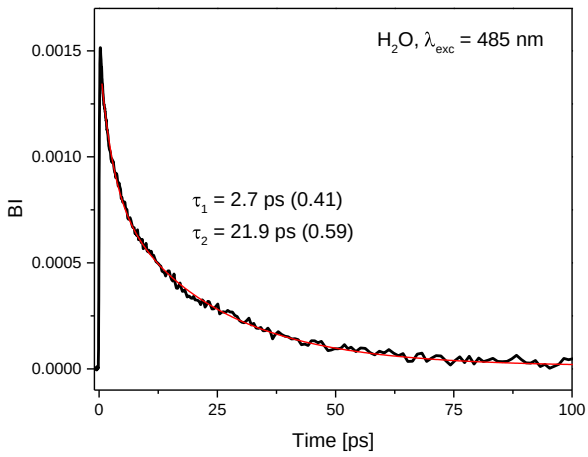

Figure S9. (A) NIR transient absorption spectra recorded with excitation at 485 nm for miraxanthin V in MeOH. (B) The determined decay-associated spectra with their respective time constants obtained by double-exponential global fit. (C) Two time constants τ_1 and τ_2 were obtained from double exponential fit of band integral: 5.1 ps (0.38) and 38.7 ps (0.62).

(A)

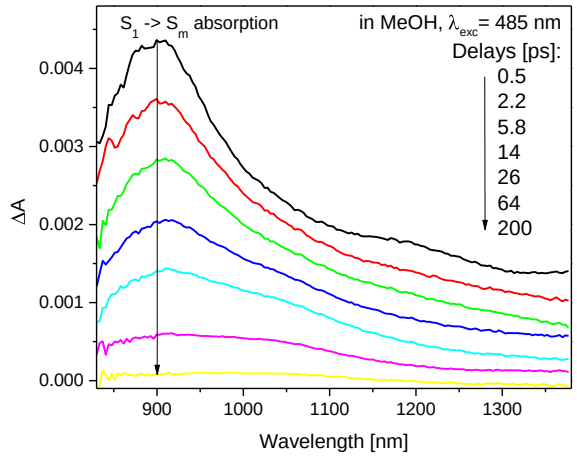

(B)

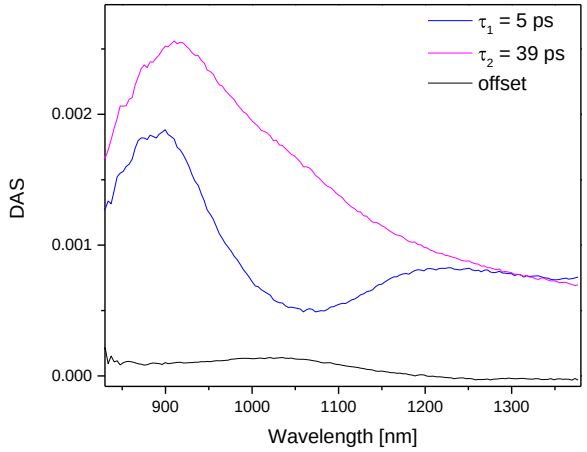

(C)

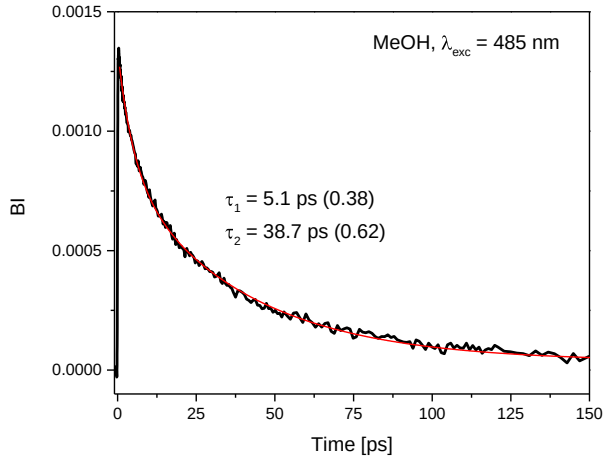

Figure S10. Dependence between miraxanthin V fluorescence quantum yield Φ_F and time constant τ_2 in various solvents.

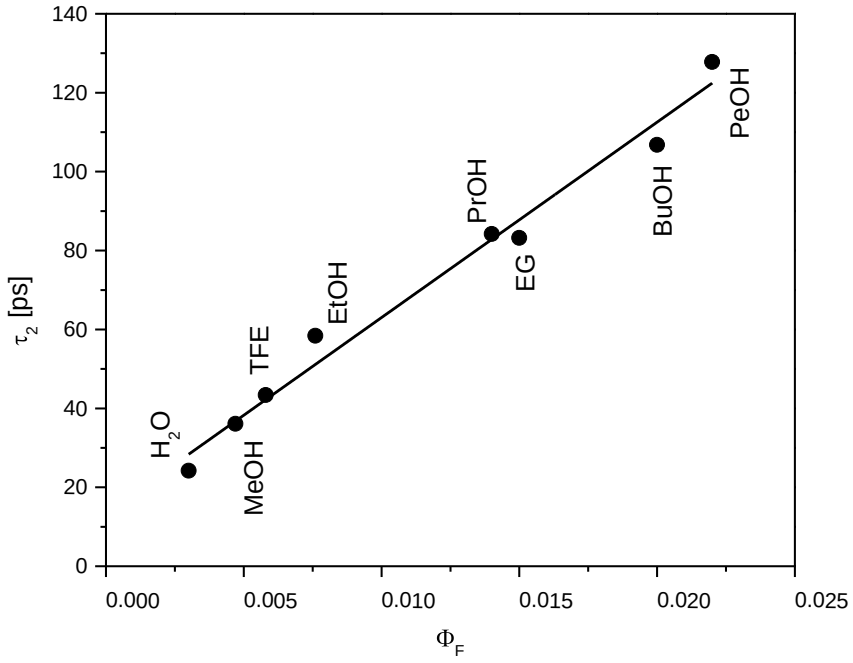

Figure S11. (A) Transient absorption spectra recorded with excitation at 298 nm for miraxanthin V in water. (B) Band Integral decays calculated over different bands. (C) The determined decay associated spectra with their respective time constants obtained by double-exponential global fit. (D) Obtained time constants and partial amplitudes. (E) Selected transient absorption kinetic traces at probe wavelengths 460 and 520 nm, normalized at delay of 5 ps, obtained with excitation at λ_{exc} = 298 nm and λ_{exc} = 480 nm.

(A)

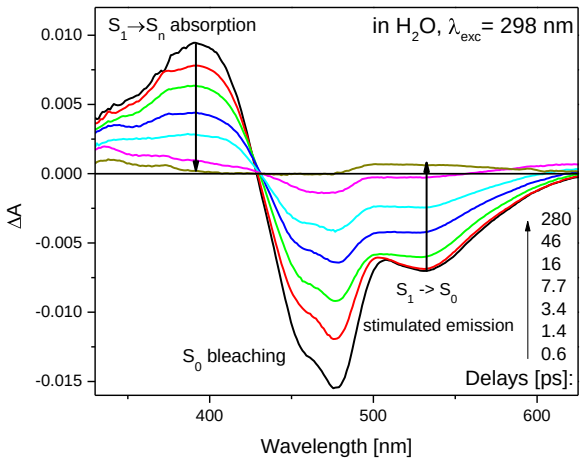

(B)

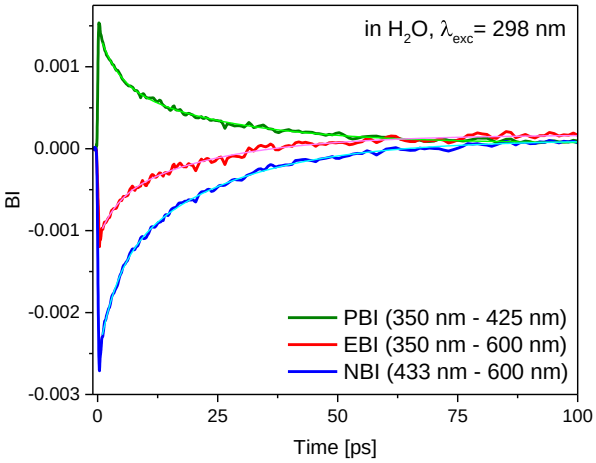

(C)

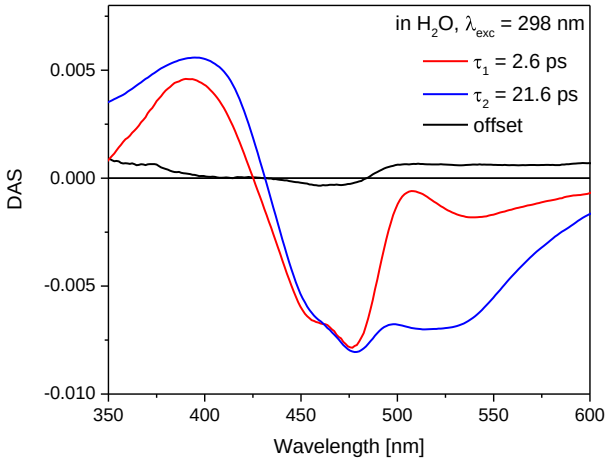

(D)

τ_1,τ_2
Positive BI 3.8 ps (0.41), 24.3 ps (0.59)
Entire BI 3.8 ps (0.33), 22.9 ps (0.67)
Negative BI 3.8 ps (0.37), 23.6 ps (0.63)
Global analysis 2.6 ps, 21.6 ps

(E)

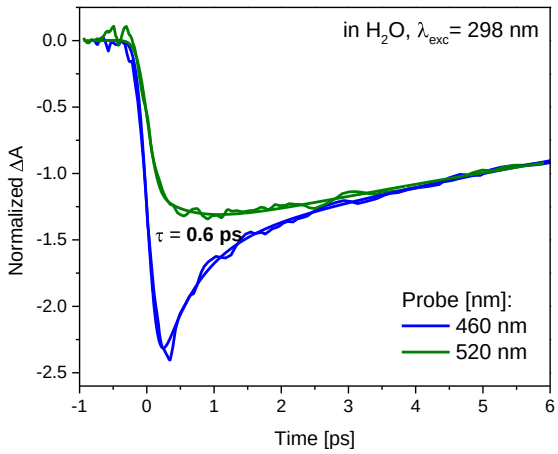

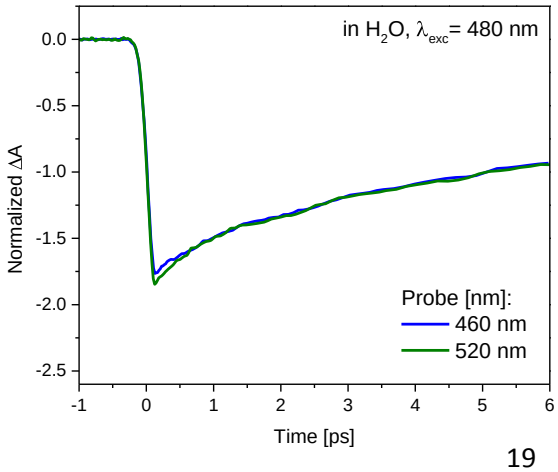

Figure S12. (A) UV-vis transient absorption spectra recorded with excitation at 480 nm for miraxanthin V in H_2O, MeOH, EtOH, TFE, PrOH, BuOH, PeOH, and EG solutions. (B) The determined decay-associated spectra with their respective time constants obtained by double-exponential global fit. (C) Band integrals fitted by double-exponential function.

(A) (B)

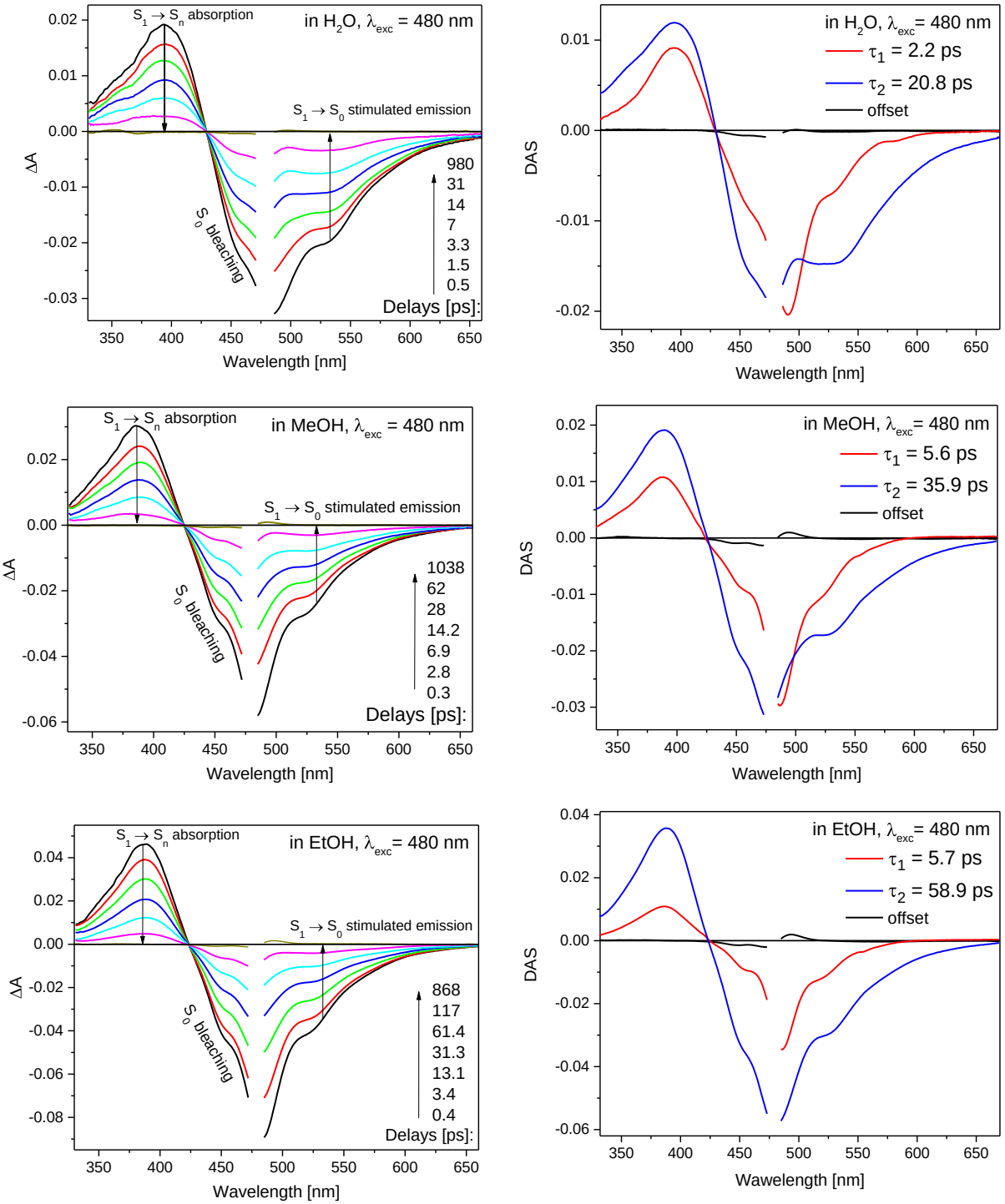

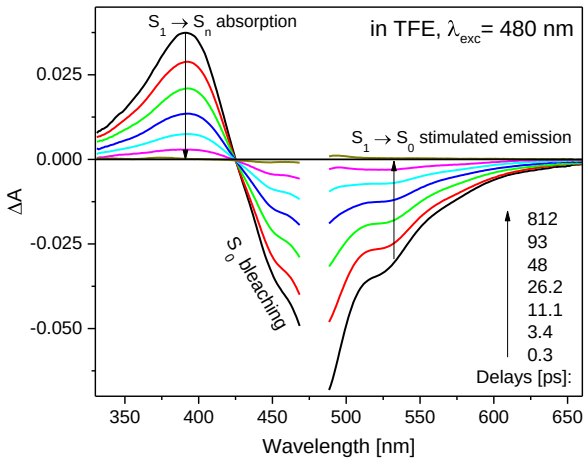
S1 → Sn absorption
in TFE, λexc= 480 nm
S1 → S0 stimulated emission
S0 bleaching
812
93
48
26.2
11.1
3.4
0.3
Delays [ps]:
ΔA
Wavelength [nm]

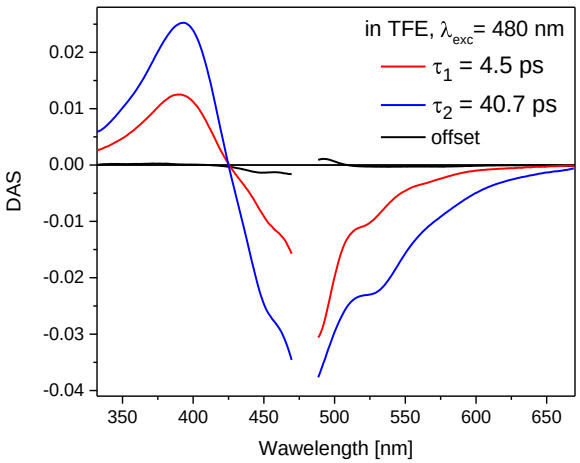
in TFE, λexc= 480 nm
τ1 = 4.5 ps
τ2 = 40.7 ps
offset
DAS
Wavelength [nm]

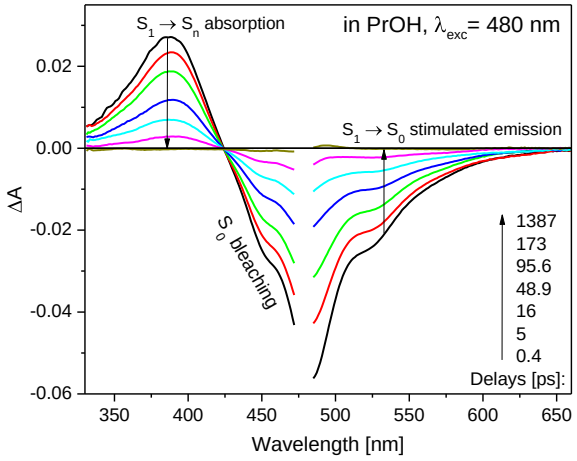
S1 → Sn absorption
in PrOH, λexc= 480 nm
S1 → S0 stimulated emission
S0 bleaching
1387
173
95.6
48.9
16
5
0.4
Delays [ps]:
ΔA
Wavelength [nm]

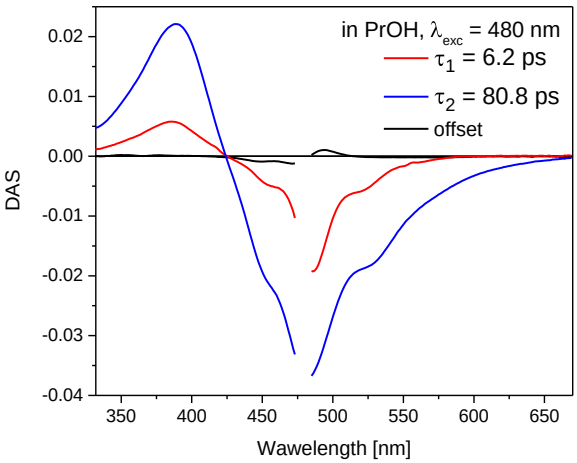
in PrOH, λexc = 480 nm
τ1 = 6.2 ps
τ2 = 80.8 ps
offset
DAS
Wavelength [nm]

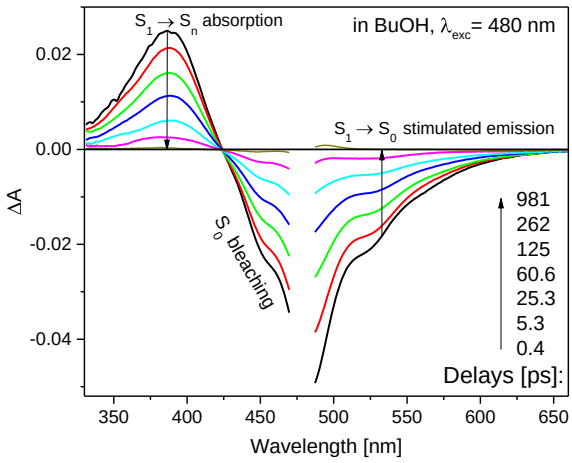
S1 → Sn absorption
in BuOH, λexc= 480 nm
S1 → S0 stimulated emission
S0 bleaching
981
262
125
60.6
25.3
5.3
0.4
Delays [ps]:
ΔA
Wavelength [nm]

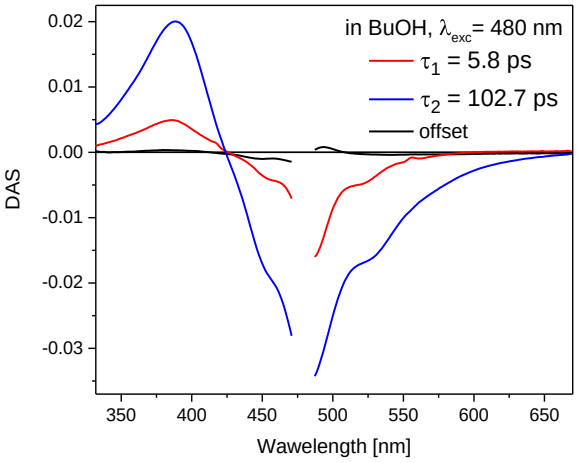
in BuOH, λexc= 480 nm
τ1 = 5.8 ps
τ2 = 102.7 ps
offset
DAS
Wavelength [nm]

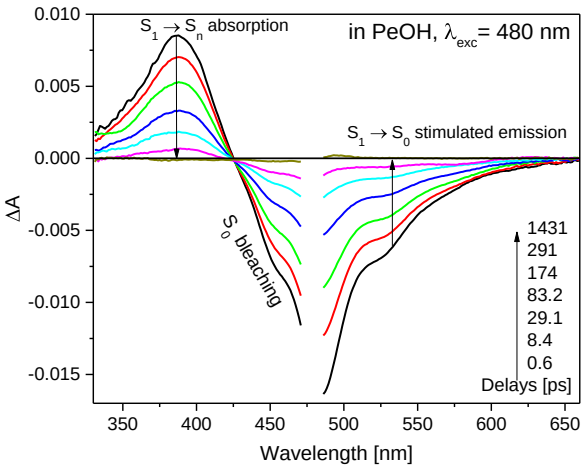
S1 → Sn absorption
in PeOH, λexc= 480 nm
S1 → S0 stimulated emission
S0 bleaching
1431
291
174
83.2
29.1
8.4
0.6
Delays [ps]
ΔA
Wavelength [nm]

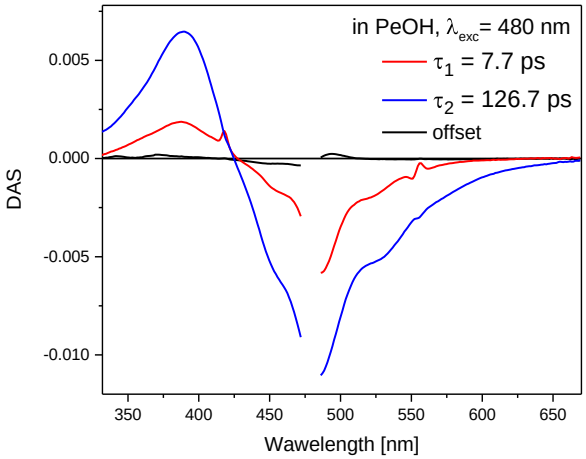
in PeOH, λexc= 480 nm
τ1 = 7.7 ps
τ2 = 126.7 ps
offset
DAS
Wawelength [nm]

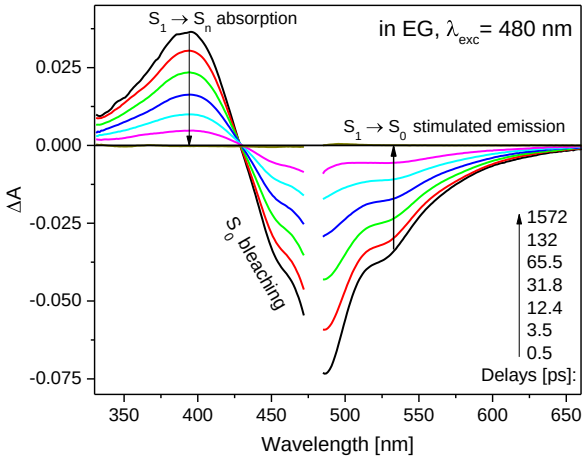
S1 → Sn absorption
in EG, λexc= 480 nm
S1 → S0 stimulated emission
S0 bleaching
1572
132
65.5
31.8
12.4
3.5
0.5
Delays [ps]:
ΔA
Wavelength [nm]

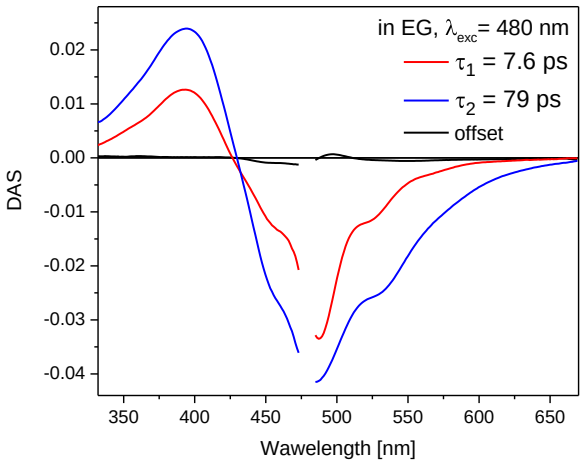
in EG, λexc= 480 nm
τ1 = 7.6 ps
τ2 = 79 ps
offset
DAS
Wawelength [nm]

(C)

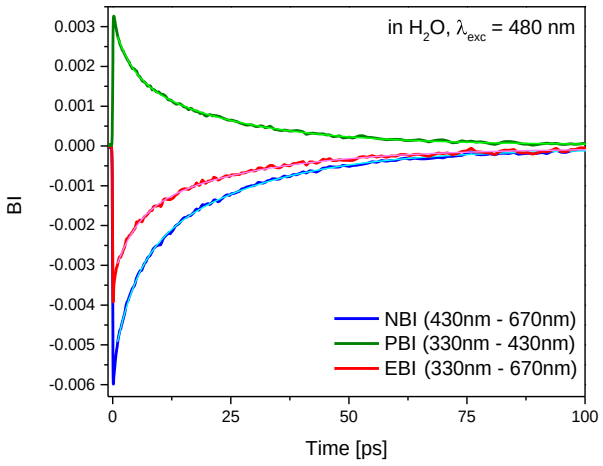
in H_2O, λ_{exc} = 480 nm
BI
Time [ps]
NBI (430nm - 670nm)
PBI (330nm - 430nm)
EBI (330nm - 670nm)

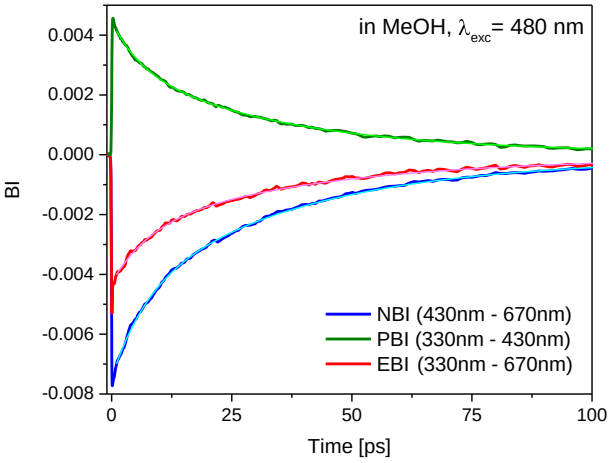
in MeOH, λ_{exc}= 480 nm
BI
Time [ps]
NBI (430nm - 670nm)
PBI (330nm - 430nm)
EBI (330nm - 670nm)

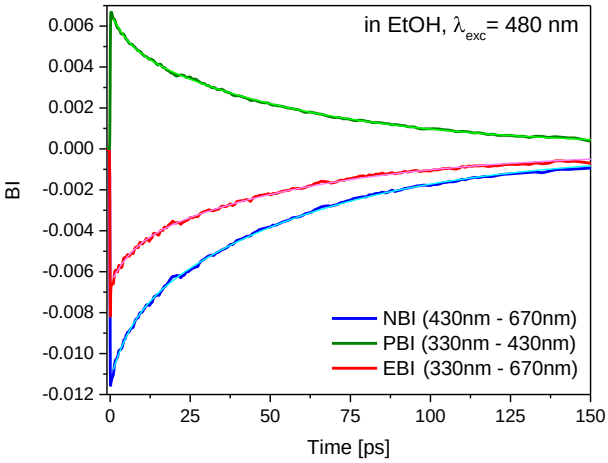
in EtOH, λ_{exc}= 480 nm
BI
Time [ps]
NBI (430nm - 670nm)
PBI (330nm - 430nm)
EBI (330nm - 670nm)

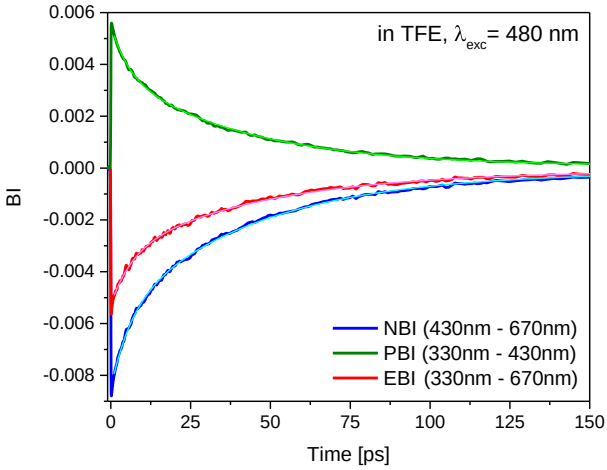
in TFE, λ_{exc}= 480 nm
BI
Time [ps]
NBI (430nm - 670nm)
PBI (330nm - 430nm)
EBI (330nm - 670nm)

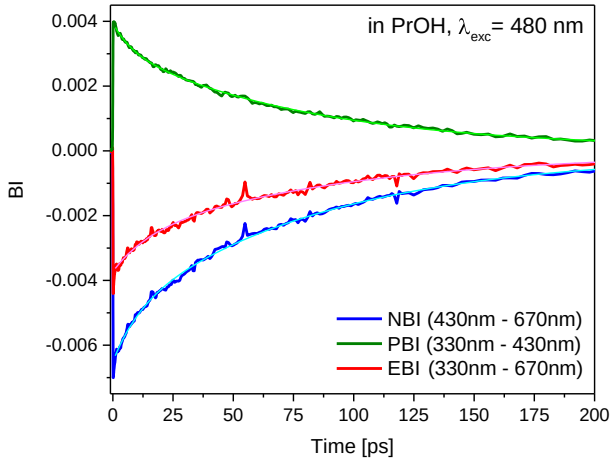
in PrOH, λ_{exc}= 480 nm
BI
Time [ps]
NBI (430nm - 670nm)
PBI (330nm - 430nm)
EBI (330nm - 670nm)

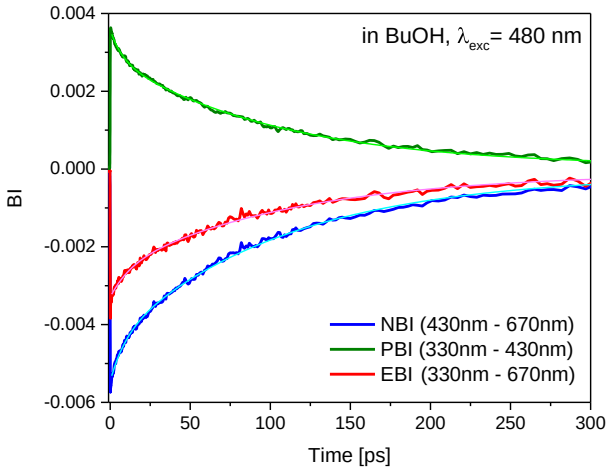
in BuOH, λ_{exc}= 480 nm
BI
Time [ps]
NBI (430nm - 670nm)
PBI (330nm - 430nm)
EBI (330nm - 670nm)

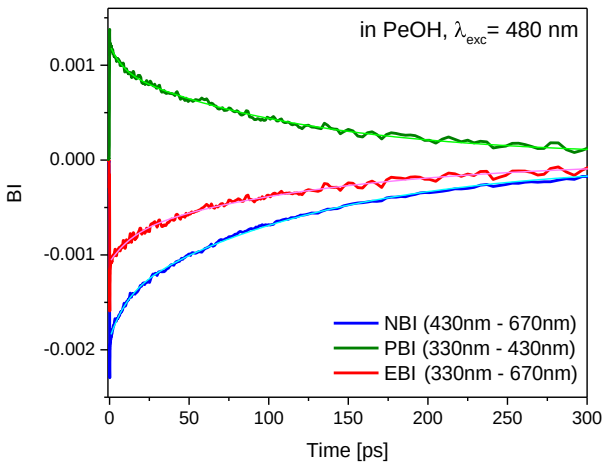
in PeOH, λ_{exc}= 480 nm
BI
Time [ps]
NBI (430nm - 670nm)
PBI (330nm - 430nm)
EBI (330nm - 670nm)

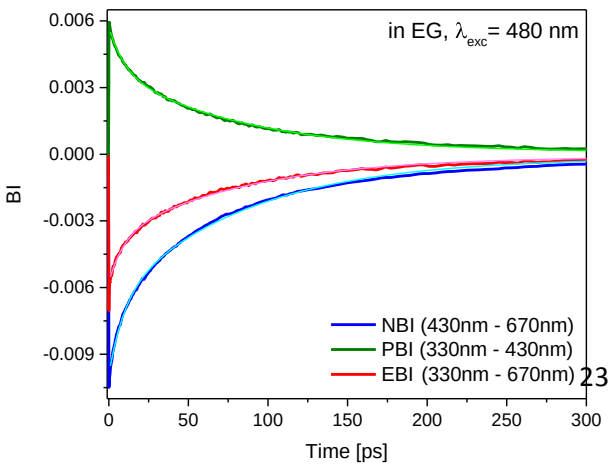
in EG, λ_{exc}= 480 nm
BI
Time [ps]
NBI (430nm - 670nm)
PBI (330nm - 430nm)
EBI (330nm - 670nm)

Figure S13. Dependence of miraxanthin V decay time constants on viscosity/temperature in methanolic solution.

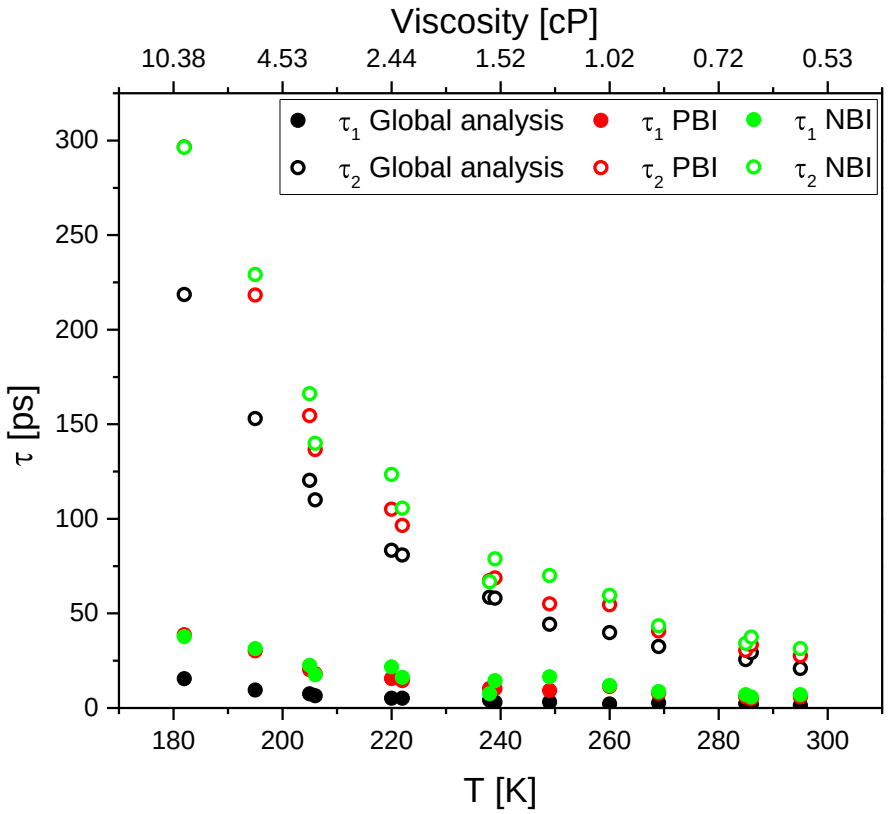

Figure S14. Surface fit for the dependence of the miraxanthin V S_1 decay rate vs. solvent viscosity and temperature.

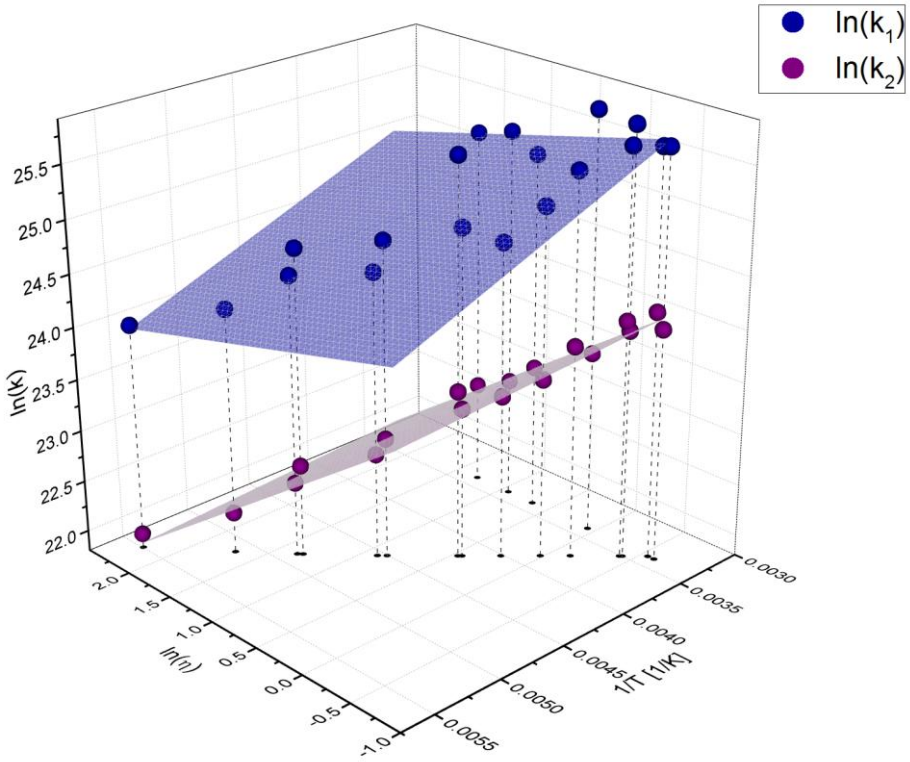

Figure S15. Equilibrium ground-state geometries of two stereoisomeric forms of miraxanthine V: ***EE*** and ***ZE*** optimized at the MP2/cc-pVDZ theory level.

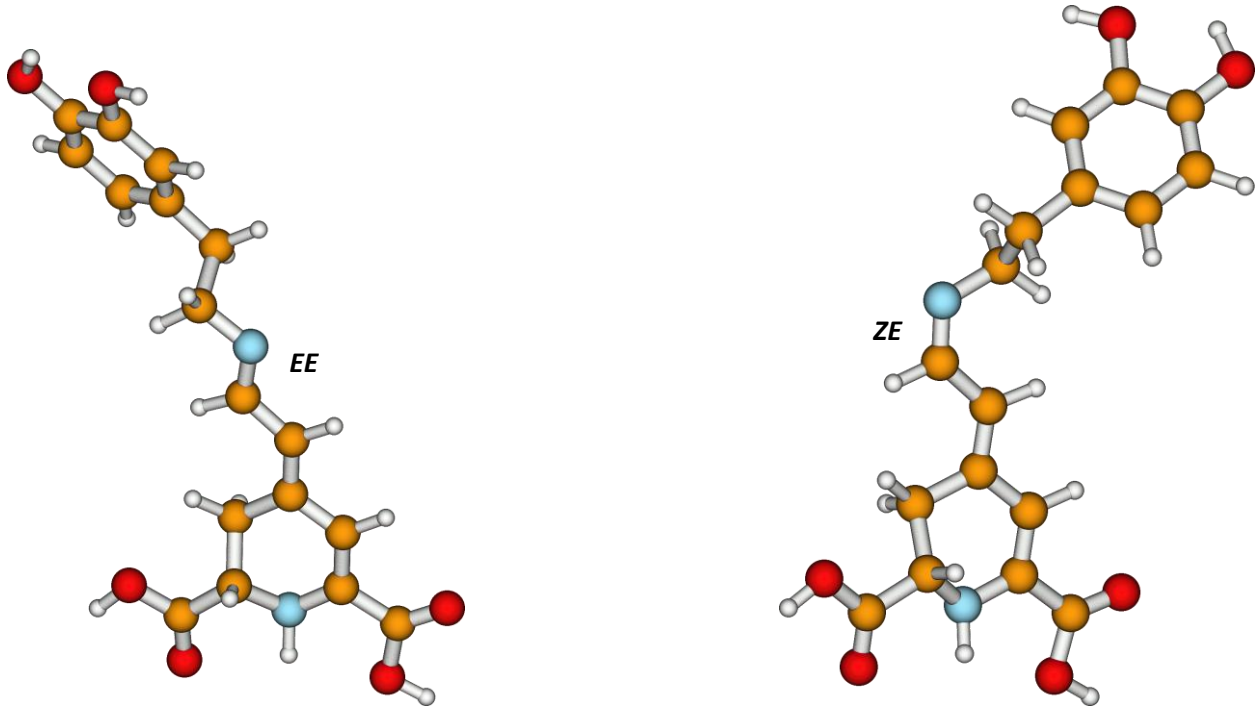

Figure S16. Potential-energy profiles of miraxanthin V in the $^1\pi\pi^*$ (blue triangles) and $^1n\pi^*$ (red squares) excited states determined at the ADC(2)/def-SV(P) level (MP2/def-SV(P) for the ground state) along the minimum energy path (solid line) in the vicinity of FC region of the ***EE*** and ***ZE*** stereoisomers. $S_0^{(\pi\pi^*)}$ (empty triangles) denotes the energy of the ground state calculated along the minimum-energy path of the appropriate excited state (dashed curves). Fluorescence energy (E_{fl}) was calculated at the ADC(2)/cc-pVDZ level.

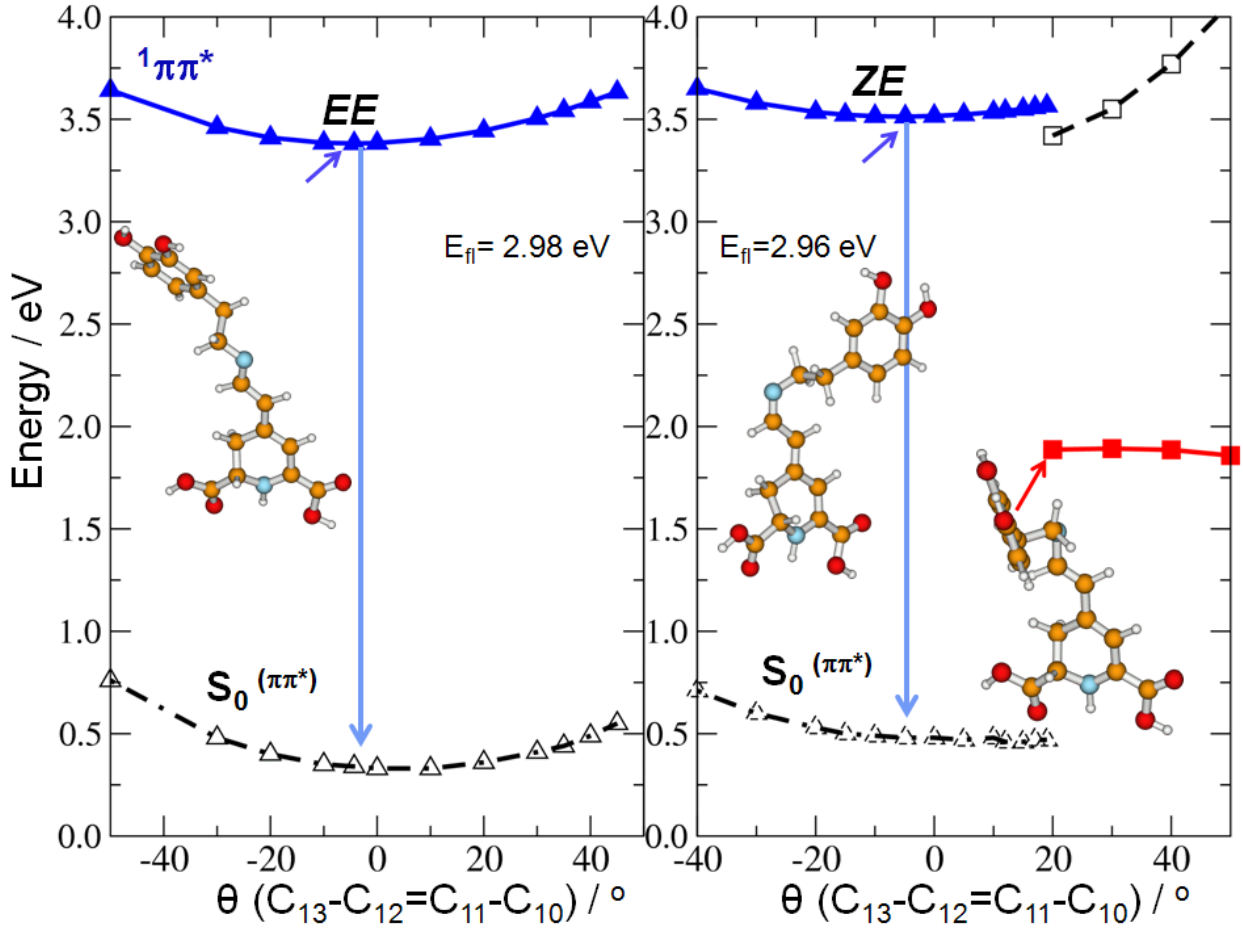

Figure S17. Potential-energy profiles of miraxanthin V in the $^{1}\pi\pi^{*}$ (blue triangles) excited state determined at the ADC(2)/def-SV(P) level (MP2/def-SV(P) for the ground state) along the minimum energy path (solid line) in the vicinity of FC region of the ***EE*** stereoisomer. $S_0^{(\pi\pi^{*})}$ (empty triangles) denotes the energy of the ground state calculated along the minimum-energy path of the $\pi\pi^{*}$ excited state (dashed curves). Fluorescence energy (E_{fl}) was calculated at the ADC(2)/cc-pVDZ level.